

Bright tripartite entanglement in triply concurrent parametric down conversion

A. S. Bradley and M. K. Olsen

ARC Centre of Excellence for Quantum-Atom Optics, School of Physical Sciences, University of Queensland, Brisbane, QLD 4072, Australia.

O. Pfister and R. C. Pooser

Department of Physics, University of Virginia, 382 McCormick Road, Charlottesville, Virginia 22904-4714, USA.

(Dated: December 2, 2024)

We show that an intracavity optical device which utilises concurrent $\chi^{(2)}$ nonlinearities can produce output beams which exhibit strong tripartite entanglement. Above threshold a significant degree of entanglement is predicted for beams with macroscopic intensities. We also demonstrate two independent ways that the system can exhibit a three mode form of the Einstein-Podolsky-Rosen paradox.

PACS numbers: 42.50.Dv,42.65.Lm,03.65.Ud,03.67.Mn

Entanglement is a property which is central to quantum mechanics, playing an important role in the Einstein-Podolsky-Rosen (EPR) paradox, quantum teleportation, quantum information and quantum cryptography [1]. Bipartite entanglement is now readily producible experimentally, and there has been some progress in the production of tripartite entangled beams, where entanglement has been obtained by mixing squeezed vacua with linear optical elements [2]. In our proposal strong entanglement is created in the nonlinear interaction itself and, as we will demonstrate, is present above the operating threshold, where the entangled outputs are macroscopically bright beams. We confirm that the output fields satisfy criteria for measurable continuous-variable tripartite entanglement [4] and derive two types of experimental EPR [5] criteria which are applicable to this system. We then show analytically and numerically that the proposed system demonstrates these properties, both above and below threshold.

A realisation of concurrent intracavity parametric down conversion in a single optical parametric oscillator (OPO) was proposed by Pfister *et al.* [6]. Different concurrent $\chi^{(2)}$ process has also been proposed by Ferraro *et al.* [7], and by Rodionov and Chirkin [8]. However, these did not use a cavity and thus would not be as suitable for our purposes. A schematic of our system is given in Fig. 1, showing the three quasi phase-matched inputs, which interact with the crystal to produce three output beams at frequencies ω_0 , ω_1 and ω_2 , with the interactions selected to couple distinct polarisations. Mode 1 is pumped at frequency and polarisation $(\omega_0 + \omega_1, y)$ to produce modes 4 (ω_0, z) and 5 (ω_1, y), mode 2 is pumped at frequency $(2\omega_1, z)$ to produce modes 5 and 6 (ω_2, y), while mode 3 is pumped at frequency $(\omega_1 + \omega_2, y)$ to produce modes 5 and 6. The Hamiltonian for the six-mode system is

$$\hat{H}_{\text{tot}} = \hat{H}_{\text{free}} + \hat{H}_{\text{pump}} + \hat{H}_{\text{int}} + \hat{H}_{\text{damp}}, \quad (1)$$

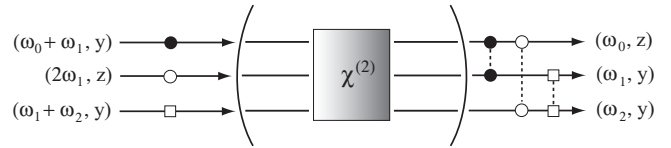


FIG. 1: Schematic of the experimental setup. Pump lasers drive three modes (denoted by dots, squares and circles), with suitable frequencies and polarisations, which are down converted to three other output modes by the crystal. Note that the physical beams will overlap in the crystal, the separation being intended here for clarity.

where the rotating frame interaction Hamiltonian is

$$\hat{H}_{\text{int}} = i\hbar(\chi_1 \hat{a}_1 \hat{a}_4^\dagger \hat{a}_5^\dagger + \chi_2 \hat{a}_2 \hat{a}_5^\dagger \hat{a}_6^\dagger + \chi_3 \hat{a}_3 \hat{a}_4^\dagger \hat{a}_6^\dagger) + \text{h.c.}, \quad (2)$$

with the χ_j representing the effective nonlinearities, and the free and damping Hamiltonians have their usual forms. The laser fields pumping the cavity are treated as classical. Following the standard procedures [9, 10] we obtain the master equation

$$\frac{\partial \hat{\rho}}{\partial t} = -\frac{i}{\hbar} [\hat{H}_{\text{pump}} + \hat{H}_{\text{int}}, \hat{\rho}] + \sum_{j=1}^6 \gamma_j \mathcal{D}_j[\hat{\rho}] \quad (3)$$

where the Lindblad superoperator $\mathcal{D}_j[\hat{\rho}] \equiv 2\hat{a}_j \hat{\rho} \hat{a}_j^\dagger - \hat{a}_j^\dagger \hat{a}_j \hat{\rho} - \hat{a}_j \hat{\rho} \hat{a}_j^\dagger$ is obtained by tracing over the density matrix for the usual zero-temperature Markovian reservoirs. We assume that all intracavity modes are resonant with the cavity, although detuning can easily be added. We will treat all of the high (low) frequency modes as having the same cavity loss rate γ (κ). In what follows we set $\gamma_1 = \gamma_2 = \gamma_3 = \gamma$, and $\gamma_4 = \gamma_5 = \gamma_6 = \kappa$, noting that the $\chi^{(2)}$ down conversion efficiencies are not necessarily identical [6].

Following the standard procedures [9], we map the master equation onto a Fokker-Planck equation for the positive-P function [11]. Note that we must use the doubled phase space of the positive-P in order to ensure positive semi-definite diffusion. One can then establish a

correspondence between stochastic amplitudes α_j (and α_j^+) and mode operators \hat{a}_j (and \hat{a}_j^\dagger) respectively, α_j and α_j^+ being independent complex variables. We then find the appropriate stochastic differential equations in Itô calculus,

$$\begin{aligned} d\alpha_1 &= (-\gamma\alpha_1 + E_1 - \chi_1\alpha_4\alpha_5) dt, \\ d\alpha_2 &= (-\gamma\alpha_2 + E_2 - \chi_2\alpha_5\alpha_6) dt, \\ d\alpha_3 &= (-\gamma\alpha_3 + E_3 - \chi_3\alpha_4\alpha_6) dt, \\ d\alpha_4 &= (-\kappa\alpha_4 + \chi_1\alpha_1\alpha_5^+ + \chi_3\alpha_3\alpha_6^+) dt \\ &\quad + \sqrt{\chi_1\alpha_1} dW_1(t) + \sqrt{\chi_3\alpha_3} dW_3(t), \\ d\alpha_5 &= (-\kappa\alpha_5 + \chi_1\alpha_1\alpha_4^+ + \chi_2\alpha_2\alpha_6^+) dt \\ &\quad + \sqrt{\chi_2\alpha_2} dW_2(t) + \sqrt{\chi_1\alpha_1} dW_1^*(t), \\ d\alpha_6 &= (-\kappa\alpha_6 + \chi_2\alpha_2\alpha_5^+ + \chi_3\alpha_3\alpha_4^+) dt \\ &\quad + \sqrt{\chi_2\alpha_2} dW_2^*(t) + \sqrt{\chi_3\alpha_3} dW_3^*(t), \end{aligned} \quad (4)$$

and also the equations obtained by interchange of α_j with α_j^+ , and $dW_j(t)$ with $dW_{j+3}(t)$. The quantum dynamics are thus generated by six independent complex Wiener increments, where the only non-vanishing correlation is

$$\overline{dW_i^*(t)dW_j(t')} = \delta_{ij}\delta(t-t') dt. \quad (5)$$

We will linearise the equations about their semi-classical solutions. We first solve for these by dropping the noise terms in Eq. 4 so that $\alpha_j^+ \rightarrow \alpha_j^*$, and solving for the steady states. We then find linearised equations for the fluctuations $\delta\boldsymbol{\alpha} = \boldsymbol{\alpha} - \boldsymbol{\alpha}^{ss}$, where $\boldsymbol{\alpha} = (\alpha_1, \alpha_1^*, \alpha_2, \alpha_2^*, \dots, \alpha_6, \alpha_6^*)^T$, which allows us to treat the system as an Ornstein-Uhlenbeck process and find relatively simple expressions for the output spectra. The resulting matrix equation is

$$d\delta\boldsymbol{\alpha} = \mathbf{A}_{ss}\delta\boldsymbol{\alpha} dt + \mathbf{B}_{ss} d\mathbf{W}, \quad (6)$$

where $d\mathbf{W}$ is a vector of independent real Wiener increments, \mathbf{B}_{ss} is the noise matrix of Eq. 4 with the steady-state values inserted, and

$$\mathbf{A}_{ss} = \begin{bmatrix} \mathbf{A}_1 & \mathbf{A}_2 \\ -(\mathbf{A}_2^*)^T & \mathbf{A}_3 \end{bmatrix}, \quad (7)$$

where $\mathbf{A}_1 = -\gamma I_6$,

$$\mathbf{A}_2 = \begin{bmatrix} -\chi_1\alpha_5 & 0 & -\chi_1\alpha_4 & 0 & 0 & 0 \\ 0 & -\chi_1\alpha_5^* & 0 & -\chi_1\alpha_4^* & 0 & 0 \\ 0 & 0 & -\chi_2\alpha_6 & 0 & -\chi_2\alpha_5 & 0 \\ 0 & 0 & 0 & -\chi_2\alpha_6^* & 0 & -\chi_2\alpha_5^* \\ -\chi_3\alpha_6 & 0 & 0 & 0 & -\chi_3\alpha_4 & 0 \\ 0 & -\chi_3\alpha_6^* & 0 & 0 & 0 & -\chi_3\alpha_4^* \end{bmatrix}, \quad (8)$$

and

$$\mathbf{A}_3 = \begin{bmatrix} -\kappa & 0 & 0 & \chi_1\alpha_1 & 0 & \chi_3\alpha_3 \\ 0 & -\kappa & \chi_1\alpha_1^* & 0 & \chi_3\alpha_3^* & 0 \\ 0 & \chi_1\alpha_1 & -\kappa & 0 & 0 & \chi_2\alpha_2 \\ \chi_1\alpha_1^* & 0 & 0 & -\kappa & \chi_2\alpha_2^* & 0 \\ 0 & \chi_3\alpha_3 & 0 & \chi_2\alpha_2 & -\kappa & 0 \\ \chi_3\alpha_3^* & 0 & \chi_2\alpha_2^* & 0 & 0 & -\kappa \end{bmatrix}. \quad (9)$$

Note that the variables in \mathbf{A}_{ss} are the steady-state solutions, α_j^{ss} , but we have omitted the superscript here for brevity. The system is stable as long as the eigenvalues of \mathbf{A}_{ss} have no positive real part. For simplicity in what follows, we will assume that all the nonlinearities are equal, i.e. $\chi_j = \chi$. This can be achieved via quasi-phase-matched interactions in periodically poled ferroelectrics [6].

If we treat all the pump fields as real, all the signal fields are also real since there is a phase condition,

$$\phi_4 + \phi_5 = \phi_4 + \phi_6 = \phi_5 + \phi_6 = 0, \quad (10)$$

which must be satisfied. As with the standard optical parametric oscillator, we find that there is an oscillation threshold at the pumping amplitude

$$E_j^{\text{th}} = \frac{\gamma\kappa}{2\chi} \quad \text{for } j \in \{1, 2, 3\}, \quad (11)$$

below which the stable solutions are $\alpha_4^{ss} = \alpha_5^{ss} = \alpha_6^{ss} = 0$, and

$$\alpha_j^{ss} = E_j/\gamma \quad \text{for } j \in \{1, 2, 3\}. \quad (12)$$

At the threshold the fluctuations are not damped and therefore a linear fluctuation analysis is not valid. If the pumping is increased further, modes 4, 5 and 6 become macroscopically occupied, while the high frequency modes do not increase further from the threshold value

$$\alpha_j^{ss} = \frac{\kappa}{2\chi} \quad \text{for } j \in \{1, 2, 3\}. \quad (13)$$

There is also a relationship between the driving fields that must be satisfied to have a steady state, which in the case of equal nonlinearities, means that all the pump amplitudes must be equal and consequently that all the signal amplitudes are equal:

$$\alpha_j^{ss} = \sqrt{(E_j - E_j^{\text{th}})/\chi} \quad \text{for } j \in \{4, 5, 6\}. \quad (14)$$

We note here that, due to the presence of the square-root, there is an ambiguity in the sign of these solutions. However, closer analysis shows that all must have the same sign, whether this is positive or negative. These above and below threshold solutions now enable us to investigate the quantum correlations of the system. We will first describe the quantities which may be measured to demonstrate that this system demonstrates true multipartite entanglement. We define quadrature operators for each mode as

$$\hat{X}_j = \hat{a}_j + \hat{a}_j^\dagger, \quad \hat{Y}_j = -i(\hat{a}_j - \hat{a}_j^\dagger), \quad (15)$$

so that $[\hat{X}_j, \hat{Y}_j] = 2i$ and the Heisenberg uncertainty principle requires $V(X_j)V(Y_j) \geq 1$, which sets the vacuum noise level. Conditions which are sufficient to demonstrate bipartite entanglement are well known [3]. These

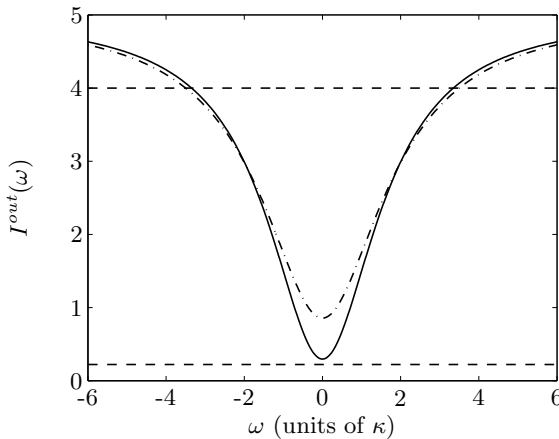


FIG. 2: Spectra for the entanglement criteria of Eq. 16, for equal pump amplitudes and nonlinearities in each mode. In all figures $\chi = 0.01$, $\kappa = 1$, $\gamma = 10$ and the pump values are $E = 0.9E^{\text{th}}$ (solid line) and $E = 1.1E^{\text{th}}$ (dash-dotted line). All quantities plotted in this article are dimensionless. The dashed lines represent the limiting zero-frequency threshold value of $2/9$ and the tripartite value of 4 , which is obviously violated.

have been generalised to tripartite entanglement by Van Loock and Furusawa [4], without making any assumptions about Gaussian statistics. Using our quadrature definitions, these conditions give a set of inequalities

$$\begin{aligned} V(\hat{X}_4 - \hat{X}_5) + V(\hat{Y}_4 + \hat{Y}_5 + \hat{Y}_6) &\geq 4, \\ V(\hat{X}_4 - \hat{X}_6) + V(\hat{Y}_4 + \hat{Y}_5 + \hat{Y}_6) &\geq 4, \\ V(\hat{X}_5 - \hat{X}_6) + V(\hat{Y}_4 + \hat{Y}_5 + \hat{Y}_6) &\geq 4, \end{aligned} \quad (16)$$

where $V(\hat{A}) \equiv \langle \hat{A}^2 \rangle - \langle \hat{A} \rangle^2$. The simultaneous violation of any two of these conditions proves genuine tripartite entanglement for the system. A semi-classical pump analysis of the interaction Hamiltonian (Eq. 2) reveals that these are the maximally squeezed quadrature combinations, so that we can expect optimal entanglement for these variables.

The Einstein, Podolsky and Rosen (EPR) paradox stems from their 1935 paper [5], which showed that local realism is not consistent with quantum mechanical completeness. As shown by Reid and Drummond [12], optical quadrature phase amplitudes have the same mathematical properties as the position and momentum originally considered by EPR. When entangled sufficiently, they allow for an inferred violation of the uncertainty principle, which is equivalent to the EPR paradox. This was experimentally demonstrated by Ou *et al.* showing clear agreement with quantum theory [14]. Following the approach of Ref. [12], we assume that a measurement of the \hat{X}_j quadrature, for example, will allow us to infer, with some error, the value of the \hat{X}_k quadrature, and similarly for the $\hat{Y}_{j,k}$ quadratures. Minimising this error, we can define *inferred variances*, the products of which demonstrate the EPR paradox when they appear to violate the

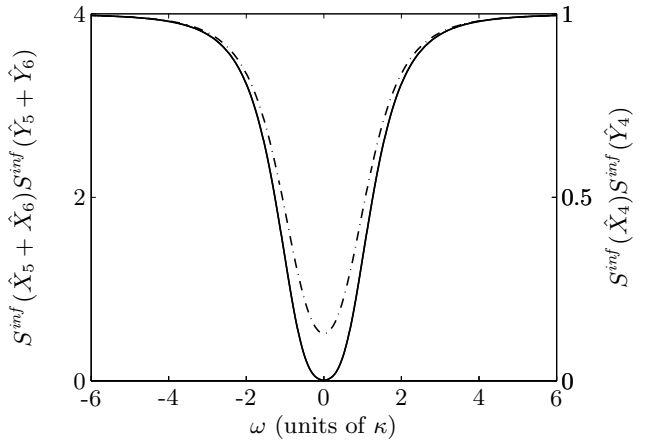


FIG. 3: Inferred output fluctuation spectra for three mode EPR correlations, from measurements on one or two modes. Below threshold ($E = 0.9E^{\text{th}}$, solid line) the spectra coincide. Above threshold ($E = 1.1E^{\text{th}}$, dash-dotted line) two mode inference gives better violation than one mode inference, but the differences are indistinguishable on this scale.

Heisenberg uncertainty principle.

Although tripartite (and therefore bipartite) entanglement is present in the system, it does not appear that a demonstration of the EPR paradox is possible via the standard two mode approach. There are two ways to demonstrate paradoxes of this nature, both involving information about all three modes. One example is to use quadrature measurements on one mode to infer values for a combination of the other two. This is mathematically equivalent to inferring, for example, the center of mass (COM) position and momenta of two particles by measurements on a third. In this case we find, using mode i to infer properties of the combined mode $j+k$, for example, the inferred variances

$$V^{\text{inf}}(\hat{X}_j \pm \hat{X}_k) = V(\hat{X}_j \pm \hat{X}_k) - \frac{[V(\hat{X}_i, \hat{X}_j \pm \hat{X}_k)]^2}{V(\hat{X}_i)}, \quad (17)$$

with similar expressions holding for the \hat{Y} quadratures. In the above $V(\hat{A}, \hat{B}) = \langle \hat{A}\hat{B} \rangle - \langle \hat{A} \rangle \langle \hat{B} \rangle$ and the i, j, k can be any of $4, 5, 6$ as long as they are all different. The product of the operator variances satisfies the inequality

$$V(\hat{X}_j \pm \hat{X}_k)V(\hat{Y}_j \pm \hat{Y}_k) \geq 4, \quad (18)$$

so that there is an inferred violation whenever

$$V^{\text{inf}}(\hat{X}_j \pm \hat{X}_k)V^{\text{inf}}(\hat{Y}_j \pm \hat{Y}_k) < 4 \quad (19)$$

which is equivalent to a three mode demonstration of the EPR paradox. Another option is to make measurements on the combined mode $j+k$ to infer properties of mode i . This leads to the inferred variances

$$V^{\text{inf}}(\hat{X}_i) = V(\hat{X}_i) - \frac{[V(\hat{X}_i, \hat{X}_j \pm \hat{X}_k)]^2}{V(\hat{X}_i \pm \hat{X}_k)}, \quad (20)$$

and a demonstration of the paradox whenever

$$V^{inf}(\hat{X}_i)V^{inf}(\hat{Y}_i) < 1. \quad (21)$$

The experimentally accessible quantities are the normally ordered fluctuation spectra corresponding to the inequalities defined above, for which the same relationships hold. These are defined as Fourier transforms of the time-normally ordered operator covariances,

$$S[\hat{A}_i, \hat{B}_j](\omega) \equiv \mathcal{FT}\langle :(\hat{A}_i(t) - \langle \hat{A}_i(t) \rangle)(\hat{B}_j(0) - \langle \hat{B}_j(0) \rangle) :\rangle, \quad (22)$$

which are related to the measurable output spectra, $S^{out}[\hat{A}_i, \hat{B}_j](\omega)$, using the standard input-output relationships for optical cavities [15]. In the results presented here, we will treat the output mirror as the only source of damping. For the inequalities of Eq. (16) we define the correlation spectra

$$I_{45}^{out}(\omega) = S^{out}[\hat{X}_4 - \hat{X}_5] + S^{out}[\hat{Y}_4 + \hat{Y}_5 + \hat{Y}_6], \quad (23)$$

and use the abbreviation $S^{out}[\hat{A}_j] \equiv S^{out}[\hat{A}_j, \hat{A}_j]$. Fluctuation spectra for $I_{46}^{out}(\omega)$ and $I_{56}^{out}(\omega)$ follow analogously. Similarly, for the variances in Eqs. 19, 21, we obtain fluctuation spectra which satisfy the same inequalities in the frequency domain.

We can find relatively simple analytic expressions for the correlations of Eq. (23) in the case where all the pump amplitudes ($E_j = E$ for $j \in \{1, 2, 3\}$) and nonlinearities are equal. Below threshold $\alpha_j^{ss} = E/\gamma = \alpha$ for $j \in \{1, 2, 3\}$ and $\alpha_j^{ss} = 0$ for $j \in \{4, 5, 6\}$. Above threshold $\alpha_j^{ss} = \kappa\gamma/2\chi = \alpha$ for $j \in \{1, 2, 3\}$ and $\alpha_j^{ss} = \beta = \sqrt{(E - E^{\text{th}})/\chi}$ for $j \in \{4, 5, 6\}$. The symmetry imposes $I_{45}^{out}(\omega) = I_{46}^{out}(\omega) = I_{56}^{out}(\omega) \equiv I_{\pm}^{out}(\omega)$ where $-(+)$ denotes the spectra below (above) threshold given by

$$I_{-}^{out}(\omega) = 5 - \frac{8\chi\kappa\alpha[7(\chi\alpha)^2 + 10\chi\kappa\alpha + 4(\omega^2 + \kappa^2)]}{[(\chi\alpha + \kappa)^2 + \omega^2][(2\chi\alpha + \kappa)^2 + \omega^2]}, \quad (24)$$

$$I_{+}^{out}(\omega) = 5 - \frac{8\chi\kappa\alpha(\omega^2 + \gamma^2)[76(\chi\beta)^4 + (\chi\beta)^2(100\gamma\kappa - 56\omega^2) + (\omega^2 + \gamma^2)(16\omega^2 + 43\kappa^2)]}{[(4(\chi\beta)^2 + 2\gamma\kappa - \omega^2)^2 + (2\kappa + \gamma)^2\omega^2][(2(\chi\beta)^2 + 3\gamma\kappa - 2\omega^2)^2 + (3\kappa + 2\gamma)^2\omega^2]}. \quad (25)$$

The solutions for these quantities are shown for pump field amplitudes of $0.9E^{\text{th}}$ and $1.1E^{\text{th}}$ in Fig. 2. There is still a strong violation of the inequalities above threshold, where the outputs are not vacuum, but are bright beams. For the pumping values shown the intracavity intensity of the three low-frequency modes is $0.1\gamma\kappa/2\chi^2$. Fig. 3 shows strong inferred violations, for the same degree of entanglement shown in Fig. 2.

In conclusion, we have shown that concurrent intracavity $\chi^{(2)}$ nonlinearities can be used to produce strongly tripartite entangled outputs, both above and below the oscillation threshold. The above threshold entanglement is found for macroscopic intensities, demonstrating a bright tripartite entanglement resource. We have also shown how this device can be used to perform multimode demonstrations of the EPR paradox.

This research was supported by the Australian Research Council and the National Science Foundation grant Nos. PHY-0245032 and EIA-0323623 and by the NSF IGERT SELIM program at the University of Virginia. We thank Peter Drummond for useful discussions.

with *Continuous Variables*, Kluwer Academic, Dordrecht, 2003; S. L. Braunstein and P. van Loock, arXiv:quant-ph/0410100.

- [2] T. Aoki *et al.*, Phys. Rev. Lett. **91**, 080404 (2003).
- [3] L.M. Duan, G. Giedke, J.I. Cirac, and P. Zoller, Phys. Rev. Lett. **84**, 2722 (2000).
- [4] P. van Loock and A. Furusawa, Phys. Rev. A **67**, 052315 (2000).
- [5] A. Einstein, B. Podolsky, and N. Rosen, Phys. Rev. **47**, 777, (1935).
- [6] O. Pfister, S. Feng, G. Jennings, R. Pooser, and D. Xie, Phys. Rev. A **70**, 020302 (2004).
- [7] A. Ferraro *et al.*, J. Opt. Soc. Am. B **21**, 1241 (2004).
- [8] A. V. Rodionov and A. S. Chirkov, JETP Lett. **79**, 253 (2004).
- [9] C.W. Gardiner and P. Zoller, *Quantum Noise*, (Springer-Verlag, Berlin, 2004).
- [10] D.F. Walls and G.J. Milburn, *Quantum Optics*, (Springer-Verlag, Berlin, 1994).
- [11] P.D. Drummond and C.W. Gardiner, J. Phys. A **13**, 2353 (1980).
- [12] M.D. Reid and P.D. Drummond, Phys. Rev. A **40**, 4493 (1989).
- [13] P.D. Drummond and M.D. Reid, Phys. Rev. A **41**, 3930 (1990).
- [14] Z.Y. Ou, S.F. Pereira, H.J. Kimble, and K.C. Peng, Phys. Rev. Lett. **68**, 3663 (1992).
- [15] C.W. Gardiner and M.J. Collett, Phys. Rev. A **31**, 3761 (1985).

[1] S. L. Braunstein and A. K. Pati, *Quantum Information*